JOURNAL OF COLLOID AND INTERFACE SCIENCE **208,** 68–80 (1998)
ARTICLE NO. CS985816

An Adsorption–Desorption-Controlled Surfactant on a Deforming Droplet

Charles D. Eggleton* and Kathleen J. Stebe†,[1]

*Department of Mechanical Engineering, UMBC, Baltimore, Maryland 21205; and †Department of Chemical Engineering, Johns Hopkins University, 3400 N. Charles Street, Baltimore, Maryland 21218

Received November 10, 1997; accepted August 19, 1998

The effects of a sorption-controlled, monolayer-forming surfactant on a drop deforming in an extensional flow are studied numerically. Scaling arguments are presented for drops of 1 cm and 1 μm, indicating the applicability of these results. For all simulations, when mass transfer is slow compared to surface convection, the insoluble limit is recovered; when mass transfer is rapid, the drop behavior is the same as that for a surfactant-free drop. For a surfactant which forms a monolayer, there is an upper bound to the surface concentration, Γ_∞. The surface tension reduction diverges as the surface concentration Γ approaches this limit, strongly altering the hydrodynamics.

The drop deformation is studied relative to a surfactant-free drop in terms of the capillary number, Ca, the ratio of characteristic viscous stresses to surface tension. In the insoluble limit, for $\Gamma \ll \Gamma_\infty$, droplets deform more than in the absence of surfactants at a given Ca and break-up at lower Ca. When stable drop shapes are attained, stagnant caps form at the drop tips. Finite surfactant mass transfer rates eliminate these caps and diminish the deformation.

For Γ approaching Γ_∞ in the insoluble limit, interfaces are strongly stressed for perturbative surface concentration gradients; Γ remains nearly uniform throughout the deformation process. Deformations are reduced at a given Ca. When stable drop shapes are attained, the surface is completely stagnated. Marangoni stresses force the surface velocity to zero to keep Γ below its upper bound. For soluble surfactants, as mass transfer rates increase, the magnitude of these stresses diminishes. Deformations change nonmonotonically with mass transfer rates and are not bounded by the limiting clean interface and insoluble limits.

The drop contribution to the volume averaged stress tensor Σ is also calculated. The axial component Σ_{zz} increases with the drop length; the radial component Σ_{rr} increases with the drop breadth. Since the deformation is strongly influenced by the surfactant concentration and the mass transfer rates, so too is Σ.

Key Words: **surfactants; Marangoni stresses; mixing; emulsions; multiphase flows; extensional flows.**

1. INTRODUCTION

Strong extensional flows are used to create a dispersion from two immiscible fluids. Surfactants are often added deliberately or are present as impurities. In order to understand the effects of surfactants on this process, the idealized flow field of a single, initially spherical droplet deforming in an extensional flow is studied, as shown in Fig. 1. The flow creates viscous stresses which deform the drop, causing it to elongate. When the surface tension resisting the stretching is sufficiently strong, the drop attains some steady shape. If not, the droplet continues to stretch until it breaks into smaller droplets. A thorough review of prior work in this problem is provided in two review articles (1, 2). This work focuses on surfactant effects in this flow; only related literature is reviewed below.

If surfactant is present in the external fluid, it will adsorb to some equilibrium surface concentration Γ_{eq} and surface tension γ_{eq}. If the surfactant remains uniformly distributed at Γ_{eq}, the process is modified solely through the surface tension reduction, and larger deformations are realized when compared to the surfactant-free case. However, the surface concentration rarely remains at its equilibrium value; rather, surface convection creates concentration gradients which alter the surface tension and therefore the stresses on the interface.

The viscous stresses scale as μG, where G is the strain rate of the applied flow. The Laplace pressure resisting deformation scales as γ_{eq}/a, where a is the initial drop radius. Their ratio defines the capillary number Ca:

$$\mathrm{Ca} = \frac{\mu G a}{\gamma_{eq}}. \qquad [1]$$

By symmetry, the tangential flow is zero at the poles and at the ring located at the drop equator. Surface convection sweeps surfactant toward the poles, where it accumulates if the mass transfer rates are slower than the surface convective flux. The distribution of surfactant strongly influences the deformations realized. If the accumulation near the drop poles is pronounced, the surface tension there will be strongly reduced. Since the normal stresses are balanced by the Laplace pressure, $2H\gamma$, the

[1] To whom correspondence should be addressed.

0021-9797/98 $25.00

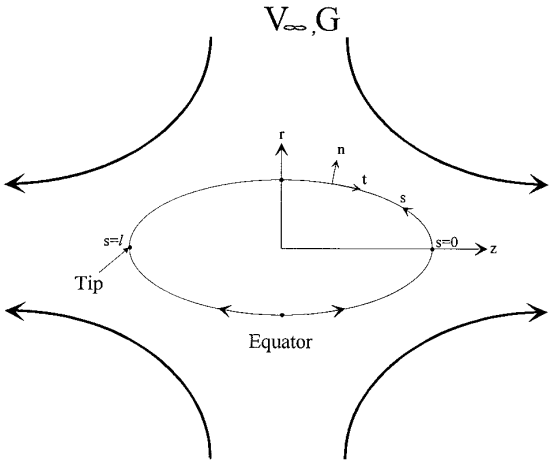

FIG. 1. A neutrally buoyant drop is suspended in an immiscible fluid of equal viscosity and subjected to a pure axisymmetric extensional flow.

poles will require a higher mean curvature $2H$ to resist a given stress jump. The drop elongates, stretching the tip region to develop this curvature. The drops are more highly deformed than the clean drop for a given Ca. If surfactant remains uniformly distributed and the surface stretches faster than mass transfer can supply surfactant, the interface becomes diluted. The surface tension becomes higher than γ_{eq} and smaller deformations result for a given Ca.

These mechanisms were identified by Stone and Leal (3), who studied insoluble surfactants in this flow. The distribution of insoluble surfactant is determined by the surface convection, which creates gradients in Γ, and surface diffusion, which eliminates these gradients. In their study, the surface tension γ was assumed linear in Γ (i.e., a 2-D ideal gas law was adopted) with a dimensionless slope $\beta_G = RT\Gamma_{eq}/\gamma_0$, where γ_0 is the surface tension of the surfactant-free interface, and RT is the product of the ideal gas constant and the temperature. Large deformations were realized when surface diffusion and β_G were weak. Small deformations were found for strong surface diffusion or large β_G, which allowed strong Marangoni stresses to retard the surface convective flux.

Milliken *et al.* (4) extended this work to address nonunity viscosity ratios and relaxations of initially deformed drops. While in most of this study the linear model was used, in one simulation, the Frumkin equation (5), which accounts for nonideal surfactant interactions and monolayer saturation, was adopted for the surface tension. However, the surface concentrations studied were too dilute for these nonlinear effects to alter the surface tension; no change in deformation was found when reported against a properly scaled Ca. Interactions were studied using the Frumkin model by Pawar and Stebe (6), who found that intermolecular attraction and repulsion can strongly alter the surface tension and the Marangoni stresses realized. Attraction strong enough to drive a surface phase transition was also studied.

Milliken and Leal (7) studied soluble surfactant in this flow, again using a linear surface tension law. For soluble surfactants, this assumption restricts the adsorption isotherm to be linear. The mass transport mechanisms of bulk diffusion, surface diffusion, surface convection, and adsorption–desorption kinetic barriers were included in the analysis. Bulk convection was neglected. A complex interplay of mass transfer and drop deformation was found as a function of these parameters. For example, drops with surfactants of strongly differing physicochemical parameters and surface velocity profiles can have the same deformations at a given Ca. It was also demonstrated that, in the limit of rapid mass transfer, the deformations and surface flows are identical to the clean interface limit. In the opposite extreme, when mass transfer is severely retarded and β_G is large, the surface velocity is strongly retarded.

The aim of this study is to understand an adsorption–desorption-controlled surfactant which obeys monolayer saturation. The major shortcoming of the commonly adopted linear model is its failure to account for the limiting area/molecule in monolayers. Eggleton *et al.* (8) recently studied the role of monolayer saturation in this problem for insoluble surfactants. Since surfactants have a limiting area per molecule, there is an upper bound to the surface concentration Γ_∞ that can be accommodated in a monolayer. This is captured in the Von Szyckowski equation

$$\pi = \gamma_0 - \gamma_{eq} = -RT\Gamma_\infty \ln\left(1 - \frac{\Gamma_{eq}}{\Gamma_\infty}\right), \qquad [2]$$

where π is the surface pressure, shown in Fig. 2 as a function of $\Gamma_\infty/\Gamma_{eq}$, the area per molecule scaled by its minimum area. In Eq. [2], γ_0 denotes the surface tension of the surfactant-free interface. (This equation can be derived using a mass action model for adsorption to the interface and the Gibb's adsorption equation (5) or using an ideal solution model for the interface (9)). There is a singularity in Eq. [2] as Γ_{eq} approaches Γ_∞. As

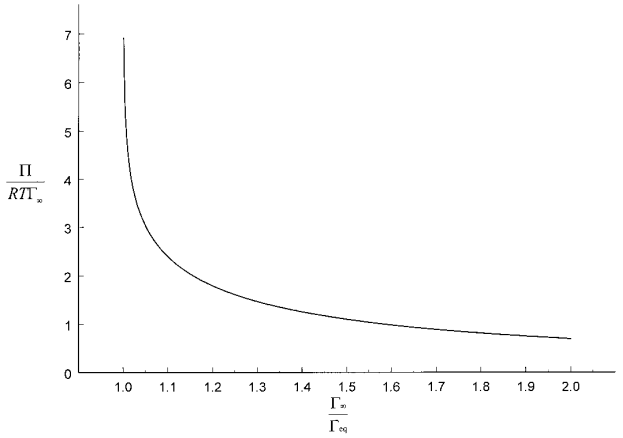

FIG. 2. Surface pressure π vs normalized area per molecule Γ_∞/Γ for the Von Szyckowski model. As the minimum area/molecule is approached, the surface pressure diverges.

is the case for all simple thermodynamic models which account for excluded area or volume effects (e.g., Van der Waal's equation), the existence of this singularity changes the response of the system to prevent the singularity from occurring. In this problem, for Γ_{eq} near Γ_∞, the highly nonlinear response of the Marangoni stress regulates the surface concentration profile so that the minimum area/molecule is not reached. For real surfactant systems, Γ_{eq} can be greater than 0.99 Γ_∞ while the surface tension remains finite; this is possible because typically, $RT\,\Gamma_\infty \ll \gamma_0$. For higher concentrations, the surfactants form self-assembled structures such as micelles in the bulk solution. These issues are not addressed in this study.

The Marangoni stresses corresponding to Eq. [2] are

$$\nabla_s\gamma = \frac{\partial\gamma}{\partial\Gamma}\nabla_s\Gamma = \frac{RT}{1-\Gamma/\Gamma_\infty}\nabla_s\Gamma, \qquad [3]$$

where ∇_s is the surface gradient operator. At dilute concentrations ($\Gamma \ll \Gamma_\infty$), the coupling between γ and Γ is weak. Strong surface concentration gradients can be created by surface convection before any Marangoni stresses develop opposing this flow. In the insoluble limit, surfactant accumulates strongly at the tip region, creating stagnant caps once the steady state shape has been attained. At higher surface concentrations (Γ approaching Γ_∞ from below), the surface tension changes strongly with Γ. Large Marangoni stresses result for perturbative Γ gradients. Surfactant remains nearly uniformly distributed during the deformation, and the deformation is dilution dominated. Furthermore, in the insoluble limit, the interfaces are nearly stagnated at steady deformation for weak surface diffusion and are strictly stagnant for zero surface diffusion. Thus, the entire range of deformation behaviors is found as a function of surface concentration.

In this paper, the work of Eggleton *et al.* is extended to account for surfactant mass transfer with the bulk. Mass transfer is considered in the adsorption–desorption-controlled limit. The stagnant caps realized on stable, deformed drops at low coverage, or stagnant surfaces found at elevated coverage, form only when surface diffusion is negligible and the surfactant is insoluble. In these circumstances, Marangoni stresses alone regulate the surface concentration profile (surface diffusion is typically weak). When the surfactant is soluble, it can desorb from the drop tip rather than accumulate there. Thus, mass transfer provides an additional mechanism to keep Γ less than Γ_∞. As the mass transfer rates increase relative to the surface convection rate, the Marangoni stress diminishes, until the interfacial flow is restored, and the deformation of a surfactant-free drop is realized. The deformations tend monotonically from the insoluble limit to the clean interface behavior.

At elevated surface concentration in the insoluble limit, Eggleton *et al.* showed that Γ varies only perturbatively from a uniform distribution, but the interface is highly stressed. For adsorption–desorption-controlled surfactants, Γ varies even less along the interface, approaching Γ_{eq} as mass transfer rates increase. Deformations agree with the insoluble result for extremely slow mass transfer and approach the clean result for rapid transport. However, they vary nonmonotonically as mass transfer rates increase and are not bounded by these two limits.

This flow field has been treated as a unit cell model for understanding the rheology of dilute emulsions. In so doing, a volume-averaged stress tensor is commonly calculated to understand the influence of the drop on the system rheology. The drop contribution to this volume-averaged stress tensor is found for this model. It is shown to be strongly influenced by the deformation of the droplet and therefore by the mass transfer rates and surface concentrations.

In most of the prior studies, the slope of the 2-D ideal gas law, β_G, was taken to be orders of magnitude larger than would be realized in experiment. Thus, variations between tip stretching and drop dilution were achieved by varying the magnitude of this quantity in a manner that cannot be realized experimentally. In Pawar and Stebe, the coupling between the (nonlinear) surface tension and surface concentration was also unrealistically strong. In Eggleton *et al.* and in this work, an effort is made to choose parameters which might be realized in experiment and to understand how surfactants with more realistic physicochemistry might effect this flow field. Results for the exaggerated coupling and the more realistic value are compared to place this prior work in context.

2. GOVERNING EQUATIONS

2.1. Mass Transfer to an Interface

A neutrally buoyant, spherical droplet of initial radius a is suspended in an initially quiescent surfactant solution of concentration C_∞. The surfactant is immiscible in the drop phase. Initially, the system is at equilibrium with surface concentration Γ_{eq}. When the straining flow is initiated with strain rate G, surfactant is redistributed by surface convection. This provokes a Marangoni stress which retards the tangential surface velocity. On the interface, the surface concentration gradient is modulated by surface diffusion. Surfactant mass transfer between the bulk and the interface also acts to restore equilibrium. The surface mass balance is given by

$$\frac{\partial\Gamma}{\partial t} + \nabla_s\cdot(\Gamma\mathbf{v}_t) + 2Hv_n\Gamma - D_s\nabla_s^2\Gamma = j_n, \qquad [4]$$

where D_s is the surface diffusivity, j_n is the mass flux from the bulk, the term containing v_t indicates the tangential surface convective flux, and the term with v_n is the dilution of the interface by dilatation. These components of the surface velocity $\mathbf{v}_s$ are defined,

$$\mathbf{v}_s = \mathbf{v}_t + \mathbf{v}_n = (\mathbf{v}_s\cdot\mathbf{t})\mathbf{t} + (\mathbf{v}_s\cdot\mathbf{n})\mathbf{n}, \qquad [5]$$

and v_t and v_n are the magnitudes of these components, **t** is the nonazimuthal unit tangent and **n** is the normal unit vector.

The flux from the bulk is controlled, in general, by both diffusion and adsorption–desorption fluxes. For a monolayer-forming surfactant, the kinetic expression for adsorption–desorption is

$$j_{a/d} = \beta C_s(\Gamma_\infty - \Gamma) - \alpha\Gamma, \qquad [6]$$

where β, α are the kinetic constants for adsorption/desorption respectively, and C_s is the concentration of surfactant in the fluid immediately adjacent to the interface. At equilibrium, this expression reduces to the Langmuir adsorption isotherm

$$x = \frac{\Gamma_{\text{eq}}}{\Gamma_\infty} = \frac{k}{1+k}; \quad k = \frac{\beta C_\infty}{\alpha}, \qquad [7]$$

where x is the fraction of surface covered by adsorbed surfactant and k is the adsorption number, the ratio of characteristic adsorption to desorption rates.

The sublayer concentration is determined by diffusion from the bulk fluid,

$$j_D = -D\mathbf{n}\cdot\nabla C|_s, \qquad [8]$$

where D is the bulk diffusion coefficient, and the concentration gradient is evaluated at the interface. The concentration C is governed by the convective–diffusion equation

$$\frac{\partial C}{\partial t} + \mathbf{v}\cdot\nabla C = D\nabla^2 C, \qquad [9]$$

which obeys the far-field conditions that C tends to C_∞ far from the droplet, and the velocity **v** tends to the far-field applied extension flow, $\mathbf{v}_\infty$. In general, both mechanisms control the flux to the interface, and so

$$j_n = j_{a/d} = j_D. \qquad [10]$$

These equations are recast in dimensionless form, according to the scales

$$\Gamma = \frac{\Gamma'}{\Gamma'_{\text{eq}}};\ C = \frac{C'}{C'_\infty};\ j_n = \frac{j'_n}{\Gamma'_{\text{eq}}G'};$$
$$\mathbf{v} = \frac{\mathbf{v}'}{G'a'};\ \mathbf{x} = \frac{\mathbf{x}'}{a'};\ t = t'G', \qquad [11]$$

where the primes indicate dimensional quantities, and the position vector defined with respect to the center of mass of the drop is denoted **x.**

The equations become

$$\frac{\partial\Gamma}{\partial t} + \nabla_s\cdot(\Gamma\mathbf{v}_t) + 2H\mathbf{v}_n\Gamma - \frac{1}{\text{Pe}_s}\nabla^2\Gamma = j_n \qquad [12]$$

$$j_{a/d} = \text{Bi}[C_s(1+k-k\Gamma) - \Gamma] \qquad [13]$$

$$j_D = -\frac{1}{\text{Pe}h}\,\mathbf{n}\cdot\nabla C|_s \qquad [14]$$

$$\frac{\partial C}{\partial t} + \mathbf{v}\cdot\nabla C = \frac{1}{\text{Pe}}\nabla^2 C. \qquad [15]$$

In these expressions, several dimensionless groups appear.

The surface Peclet and bulk Peclet numbers, respectively, are defined,

$$\text{Pe}_s = \frac{Ga^2}{D_s}; \quad \text{Pe} = \frac{Ga^2}{D}, \qquad [16]$$

where Pe is the characteristic convective flux to diffusion flux and Pe_s is the characteristic surface convective flux to surface diffusion flux.

The dimensionless adsorption depth is defined:

$$h = \frac{\Gamma_{\text{eq}}}{C_\infty}\frac{1}{a} = \frac{\beta\Gamma_\infty}{\alpha a}\frac{1}{1+k}. \qquad [17]$$

This is the characteristic depth beneath the interface diluted by surfactant adsorption. Note that this depth decreases as concentration (k) increases.

Finally, the Biot number is the ratio of characteristic desorptive to surface convective time scales:

$$\text{Bi} = \frac{\alpha}{G}. \qquad [18]$$

The surfactant distribution is adsorption–desorption controlled when the desorption flux is slow compared to the diffusion flux. This requires that the ratio $\text{Bi}(\text{Pe}h) \ll 1$. The applicability of this result to drops of radius 1 μm and 1 cm is discussed along with the results.

In this limit, concentration gradients in the bulk become negligible. The surface mass balance is modified to reflect that C is unity everywhere:

$$\frac{\partial\Gamma}{\partial t} + \nabla_s\cdot(\Gamma\mathbf{v}_t) - \frac{1}{\text{Pe}_s}\nabla_s^2\Gamma + 2H\Gamma\mathbf{v}_n = \text{Bi}(1+k)(1-\Gamma). \qquad [19]$$

For small Bi, the surfactant will behave as an insoluble layer. For Bi sufficiently large, the interface can remain in equilibrium with the bulk.

2.2. Hydrodynamics

The equations governing the flow field are stated here in dimensionless form. In addition to the scales adopted in Eq. [11], the following variables are defined,

$$p_i = \frac{p_i'}{\gamma_{eq}'/a'}; \quad \underline{\mathbf{T}} = \frac{\underline{\mathbf{T}}'}{\mu' G'}; \quad \gamma = \frac{\gamma'}{\gamma_{eq}'}, \tag{20}$$

where p_i is the pressure in either the external ($i = 1$) or drop ($i = 2$) phase, and $\underline{\mathbf{T}}$ is the viscous stress tensor. The external flow field $\mathbf{v}_1$ must agree with the applied flow field far from the droplet:

$$\lim_{x\to\infty} \mathbf{v}_1 = \mathbf{v}_\infty = \begin{bmatrix} -1 & 0 & 0 \\ 0 & -1 & 0 \\ 0 & 0 & 2 \end{bmatrix} \cdot \mathbf{x}. \tag{21}$$

At the interface, velocities are continuous and equal to the surface velocity

$$\mathbf{v}_1 = \mathbf{v}_2 = \mathbf{v}_s. \tag{22}$$

The kinematic condition at the interface is

$$\frac{d\mathbf{x}_s}{dt} = \mathbf{v}_n, \tag{23}$$

where the vector $\mathbf{x}_s$ is the position of a Lagrangian point on the interface. The stress balance requires

$$[[p]] + \mathrm{Ca}[[\mathbf{n} \cdot \underline{\mathbf{T}}]] = -\frac{Ex}{1 - x\Gamma} \nabla_s \Gamma + 2H\gamma\mathbf{n}, \tag{24}$$

where [[ ]] indicates a jump condition at the interface, and γ is given by

$$\gamma = \frac{\gamma_0}{\gamma_{eq}} + E[\ln(1 - \Gamma x)]; \quad \text{where } \frac{\gamma_0}{\gamma_{eq}} = 1 - E \ln(1 - x). \tag{25}$$

In this expression,

$$E = \frac{RT\Gamma_\infty}{\gamma_{eq}} \tag{26}$$

is the elasticity number, a measure of the sensitivity of the surface tension to surfactant adsorption.

Assuming creeping flow, both the drop and external fluid obey Stokes' equations. For an axisymmetric flow, Stokes equations can be recast as a line integral for v_s,

$$\mathbf{v}_s(\mathbf{x}_s) = \mathbf{v}_\infty(\mathbf{x}_s) - \frac{1}{8\pi} \int_{s=0}^{s=1} \underline{\mathbf{M}}(\mathbf{x}_s, \zeta) \cdot (2H\gamma\mathbf{n} + \nabla_s\gamma)(\zeta) ds(\zeta), \tag{27}$$

where $\underline{\mathbf{M}}$ is the axisymmetric Green's function for Stokes' flow (10) and ζ is an integration variable along the interface (see Fig. 1). Given the far-field velocity and the stress jump at any location along the interface, the surface velocity can be found.

Using a quasi-static approach, Eq. [27] is solved for a given surface concentration distribution. The interface location is then updated according to Eq. [23], and its shape is used to find curvatures, and the unit vectors **n** and **t.** Given this information and the velocity field, the surfactant is redistributed according to Eq. [19], and the stress balance at the interface is updated using Eqs. [24] and [25]. Equation [27] is then solved again. This process continues until v_n tends to zero or no steady shape can be attained. The details are discussed in Pawar and Stebe (6).

In order to isolate the strain rate in the capillary number, Λ and B are defined,

$$\mathrm{Pe}_s = \mathrm{Ca}\Lambda; \quad \mathrm{Bi} = \frac{B}{\mathrm{Ca}}, \tag{28}$$

where

$$\Lambda = \frac{\gamma_{eq} a}{\mu D_s}; \quad B = \frac{\alpha\mu a}{\gamma_{eq}}. \tag{29}$$

The groups Λ and B are fixed for a given surfactant solution and drop fluid. By studying the behavior of the drop at fixed B and Λ as a function of Ca, the impact of increasing strain rate on a drop of given physicochemistry can be understood. Recall, however, that the impact of solubility is determined by the ratio of the adsorption–desorption and the convective rate, Bi.

The governing equations are integrated using an arc-angle formulation. The profiles for Γ, γ, v_t, etc., are all reported as a function of arclength s, which varies from 0 to l, where l is a dimensionless contour length measured from one drop "tip" to the other. Initially, the contour length l is equal to π and increases from this value as the drop elongates.

2.3. Parameter Values Adopted in the Numerical Simulations

The elasticity number E is a measure of the sensitivity of the surface tension to the surface concentration. Using Γ_∞ of 2×10^{-10} mol/cm^2, $\gamma_0 = 72$ dyne/cm, and γ_{CMC} of 30 dyne/cm, the range of values for E can be estimated at T = 22C to be 0.1–0.2; significantly less than unity. Here, as in Eggleton *et al.*, the value of 0.2 is adopted. An E value of 8.0 was adopted in Pawar and Stebe, overestimating this sensitivity. A similar overestimation was made in the studies in which the linear

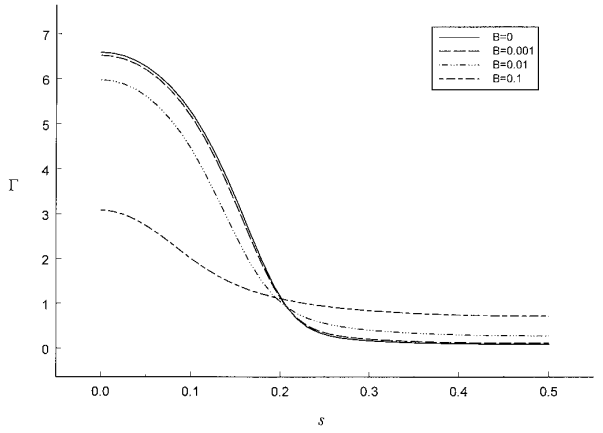

FIG. 3. The surface concentration profile Γ at Ca = 0.04 for $x = 0.1$. Results are presented for $B = 0$ (insoluble), 10^{-3}, 10^{-2}, and 0.1. All results for $\Lambda = 10^3$.

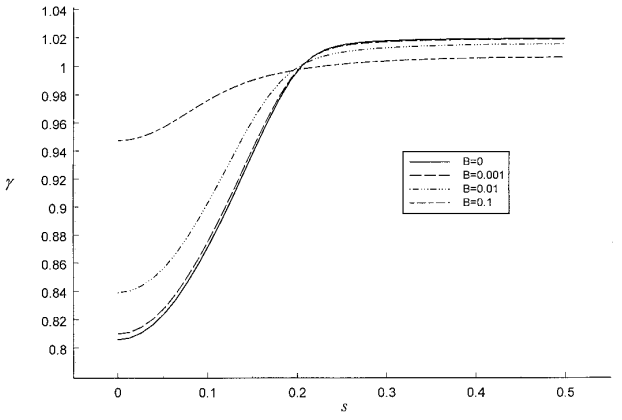

FIG. 4. The surface tension profile γ at Ca = 0.04 for $x = 0.1$. Results are presented for $B = 0$ (insoluble), 10^{-3}, 10^{-2}, and 0.1. All results for $\Lambda = 10^3$.

adsorption isotherm was adopted. Expanding the surface tension, Eq. [25], in small $x\Gamma$, and keeping only linear terms, the 2-D ideal gas law is recovered:

$$\gamma = \frac{\gamma_0}{\gamma_{eq}} - Ex\Gamma = 1 - \frac{\beta_G}{1 - \beta_G}\Gamma. \qquad [30]$$

This approximation is valid only for $x \ll 1$; therefore the slope $Ex = \beta_G/(1 - \beta_G) \ll 0.2$. However, values for β_G ranging from 0.3 to 0.85 were adopted in studies by Leal and collaborators. In order to comment on the effects of this overestimation on the results obtained, the deformation of a droplet as a function of Ca and B for $x = 0.5$ is compared for two E values ($E = 0.2$ and $E = 8.0$). For all of the other simulations, E was held fixed at 0.2. The parameter B ranges from 10^{-5} to 1. The group Λ can be estimated to be 6×10^4 for emulsion-sized drops, 6×10^8 for drops with radius of 1 cm. In our study, Λ is assumed to be 1000.

3. RESULTS AND DISCUSSION

3.1. Low Concentration Results

The surface concentration, surface tension, Marangoni stress, and tangential velocity profiles for a stable droplet at Ca of 0.04 are presented in Figs. 3–6, respectively. Consider first the case of an insoluble surfactant present on the interface at low concentrations (i.e., the fractional coverage of the interface $x = 0.1$). Initially, the system is at rest and the surfactant is uniformly distributed on the drop interface. The flow is initiated and surfactant is swept along the interface. According to Eq. [24], the Marangoni stresses resisting this flux are weak. Strong surface concentration gradients develop, until a Marangoni stress develops resisting further accumulation the region of the drop tip. At steady state for infinite Λ (i.e., negligible surface diffusion), the steady state mass balance is

$$\nabla_s \cdot (\Gamma \mathbf{v}_t) = \mathrm{Bi}(1 + k)(1 - \Gamma). \qquad [31]$$

For insoluble surfactants, Bi = 0; Eq. [31] requires that $\Gamma v_t = 0$, i.e., the droplet interface is divided into surfactant-rich, stagnated regions and surfactant-free, mobile regions. The Marangoni stress determines the Γ profile, and therefore the division between mobile and stagnant regions. For finite, large Λ, the sharp demarcation of surfactant-free and surfactant-rich regions is modulated by surface diffusion. The surface velocity remains significantly retarded near the drop tips and faster near the equator. For a soluble surfactant, Bi = B/Ca is finite, and the mass balance no longer dictates stagnant cap formation. Mass transfer with the bulk diminishes the surface concentration gradients realized. For Bi sufficiently large, the surface concentration profile approaches its equilibrium value, and the surface velocity is restored to that of a surfactant-free droplet.

The droplet deformation Df = $(L - b)/(L + b)$, where L

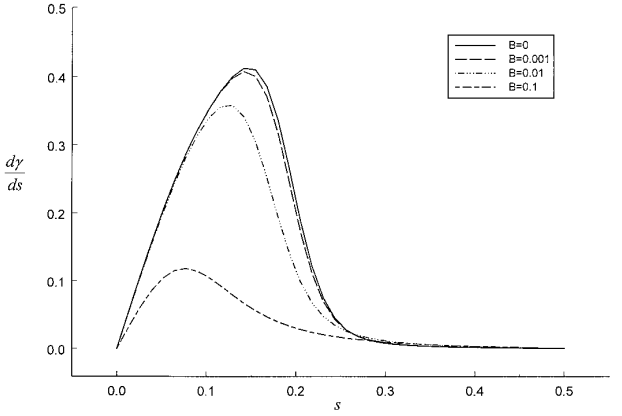

FIG. 5. The Marangoni stress profile at Ca = 0.04 for $x = 0.1$. Results are presented for $B = 0$ (insoluble), 10^{-3}, 10^{-2}, and 0.1. All results for $\Lambda = 10^3$.

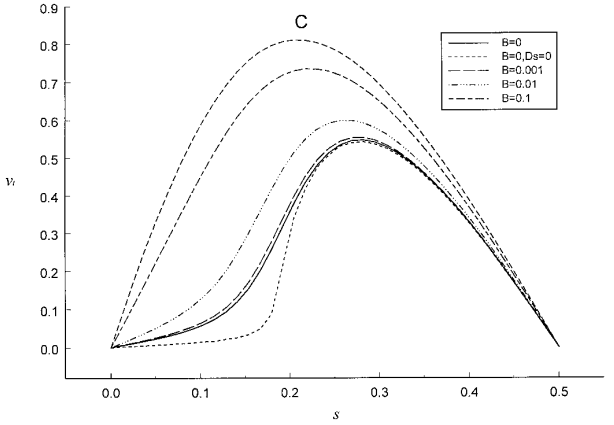

FIG. 6. The tangential surface velocity v_t profile at Ca = 0.04 for x = 0.1. Results are presented for a clean interface, $B = 0$ (insoluble), 10^{-3}, 10^{-2}, and 0.1 for $\Lambda = 10^3$; the insoluble result is also shown for conditions that correspond to stagnant cap formation, (i.e., $\Lambda = \infty$ or $D_s = 0$).

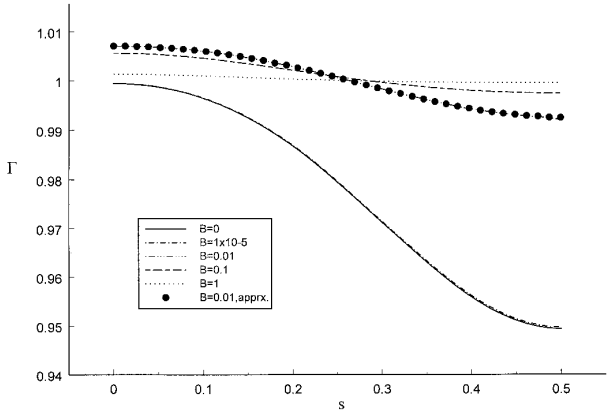

FIG. 8. The surface concentration profile Γ at Ca = 0.04 for x = 0.99. Results are presented for $B = 0$ (insoluble), 10^{-5}, 10^{-2}, 0.1, and 1. All results for $\Lambda = 10^3$. The bold dots indicate results obtained using the approximate mass balance for $B = 0.01$, Eq. [33].

is the drop length and b is the breadth, is reported in Fig. 7. For insoluble surfactant, B = 0, the surface tension is strongly reduced in the region of the drop tip. The stable drop shape is more highly deformed than the surfactant-free drop. For B small enough, the deformations superpose with those realized for an insoluble surfactant. As B increases, mass transfer eliminates the strong local reduction in γ, and the tip stretching diminishes, until, at elevated B, the deformation realized for a clean droplet is recovered. The deformations are bounded above by the insoluble results and below by the clean interface results, tending monotonically from one limit to the other as B increases. The droplet becomes unstable for Ca lower than the clean interface result; this destabilization decreases as B increases.

For $x = 0.1$, the adsorption number k is roughly 0.1 as well. Initially, Γ is uniform and there are no Marangoni stresses at the interface. When the straining flow is initiated, the Marangoni stress is of magnitude $Ex\nabla_s\Gamma/(1 - x) = 0.02E\nabla_s\Gamma$. The elimination of the Γ gradients by mass transfer allows the clean interface behavior to be recovered. This occurs for $B = 0.1$, for which the Biot number Bi = B/Ca ranges from 10 to 1.66; kBi ranges from 1 to 0.166. Recall that Bi is the ratio of the desorption rate to the surface convection rate; kBi is the ratio of the adsorption rate to the surface convection rate. At this low surface concentrations, these values are rapid enough to force gradients in Γ to be sufficiently small that the Marangoni stresses do not alter the deformation.

3.2. Elevated Concentration Results

The Γ, γ, Marangoni stress, and surface velocity profiles for stable drop shapes at Ca = 0.04 are presented in Figs. 8–11, respectively, for a fractional surface coverage $x = 0.99$. For soluble surfactants, this corresponds to an elevated bulk concentration, for which k is roughly 100.

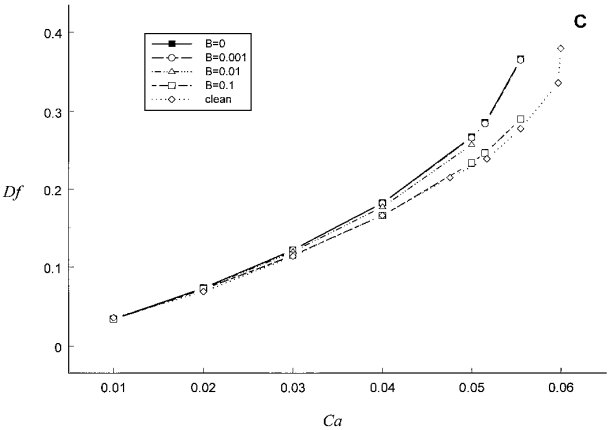

FIG. 7. The deformations Df as a function of Ca for $x = 0.1$. Results are presented for a clean interface, $B = 0$ (insoluble), 10^{-3}, 10^{-2}, and 0.1. All results for $\Lambda = 10^3$.

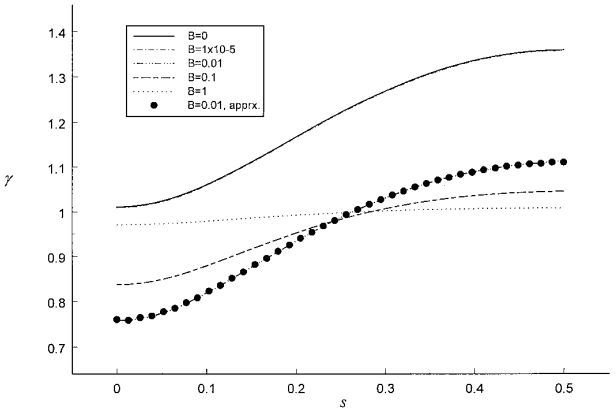

FIG. 9. The surface tension profile γ at Ca = 0.04 for $x = 0.99$. Results are presented for $B = 0$ (insoluble), 10^{-5}, 10^{-2}, 0.1, and 1. All results for $\Lambda = 10^3$. The bold dots indicate results obtained using the approximate mass balance for $B = 0.01$, Eq. [33].

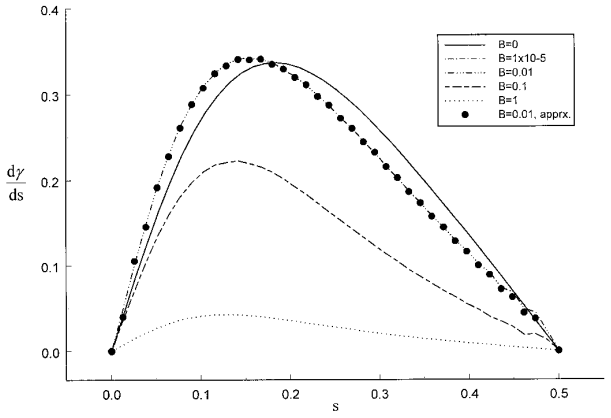

FIG. 10. The Marangoni stress profile at Ca = 0.04 for $x = 0.99$. Results are presented for $B = 0$ (insoluble), 10^{-5}, 10^{-2}, 0.1, and 1. All results for $\Lambda = 10^3$. The bold dots indicate results obtained using the approximate mass balance for $B = 0.01$, Eq. [33].

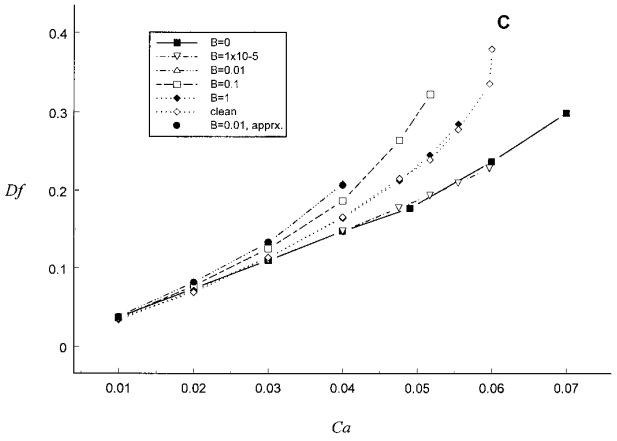

FIG. 12. The deformations Df as a function of Ca for $x = 0.99$; C indicates the surfactant-free case. Results are presented for $B = 0$ (insoluble), 10^{-5}, 10^{-2}, 0.1, and 1. All results for $\Lambda = 10^3$. Approximate mass balance results (obtained for $B = 0.01$) superpose with the full solution.

Consider first the insoluble results. For $B = 0$, Eq. [31] requires that steady state v_t be zero if Γ is nonzero. According to Eq. [24], the Marangoni stresses are significant even for perturbative surface concentration gradients. Thus, Γ remains nearly uniform, and yet the surface is highly stressed. The tangential velocity is strictly zero for infinite Λ and is nearly stagnated for Λ of 1000. The interface dilutes as the drop deforms causing the surface tension γ to increase above its equilibrium value. Smaller deformations result at a given Ca.

In the insoluble limit, Marangoni stresses are the sole mechanism to force Γ to remain less than Γ_∞ at the drop tip. However, as B increases from zero, mass transfer competes to regulate Γ. Surfactant desorbs from the drop tips and is supplied at the drop equator to restore surface equilibrium. The Marangoni stresses diminish. The dilution of the interface becomes less pronounced, and Γ remains not only nearly uniform, but approaches its equilibrium value.

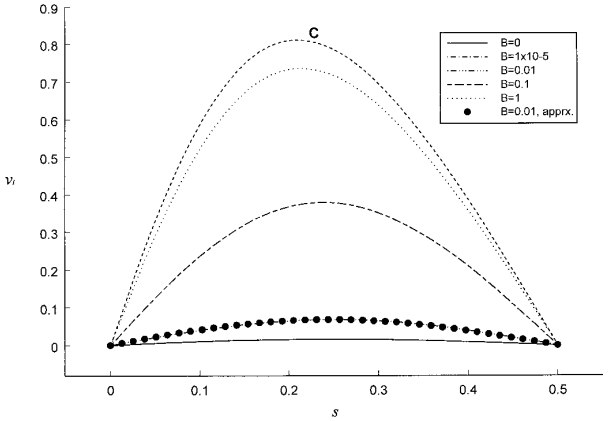

FIG. 11. The tangential surface velocity v_t profile at Ca = 0.04 for $x = 0.99$. Results are presented for a clean interface, $B = 0$ (insoluble), 10^{-5}, 10^{-2}, 0.1, and 1. All results for $\Lambda = 10^3$. The bold dots indicate results obtained using the approximate mass balance for $B = 0.01$, Eq. [33].

The deformations Df as a function of B are shown in Fig. 12. For slow mass transfer, the deformations are smaller than the clean drop. As B increases, the adsorption rate relative to surface convection (which goes as kBi) is faster than the desorption rate to surface convection ratio (which goes as Bi). Surfactant is supplied to the equator faster than it is removed from the drop tips. A Γ profile develops with accumulation near the tips, but little depletion near the equator. Therefore, the drop deforms more than the clean interface case at moderate B. Finally, for large B, Γ becomes uniform at its equilibrium value. The Marangoni stresses are eliminated, and the clean interface result is recovered. Therefore, the drop deformation varies nonmonotonically as B increases, and these deformations are not bounded by the insoluble and clean interface results.

Finally, surfactant adsorption can either stabilize or destabilize the drop against break-up, depending upon the rate of surfactant mass transfer. For mass transfer rates that are sufficiently slow (e.g., $B = 10^{-5}$) the drop is stabilized against break-up. However, for B fast enough ($B \geq 0.1$) the drop was destabilized; i.e., the critical Ca was less than that of the clean drop.

For $x = 0.99$, the adsorption number k is roughly 100. The droplet initially has no Marangoni stresses, and Γ is initially uniform. When the straining flow is initiated, the Marangoni stress is of magnitude $Ex\nabla_s\Gamma/(1 - x)$, or $20\nabla_s\Gamma$. The sensitivity of the interface to $\nabla_s\Gamma$ is orders of magnitude higher than in the low coverage case. Thus, $\nabla_s\Gamma$ must be smaller and mass transfer more rapid in order that clean interface deformations be recovered. This occurs for $B = 1$, for which the Biot number Bi $= B/\mathrm{Ca}$ ranges from 100 to 16.6; kBi ranges from 10^4 to 1.66×10^3. Thus, adsorption and desorption must be orders of magnitude more rapid at high coverage to eliminate Marangoni stresses than for low coverage.

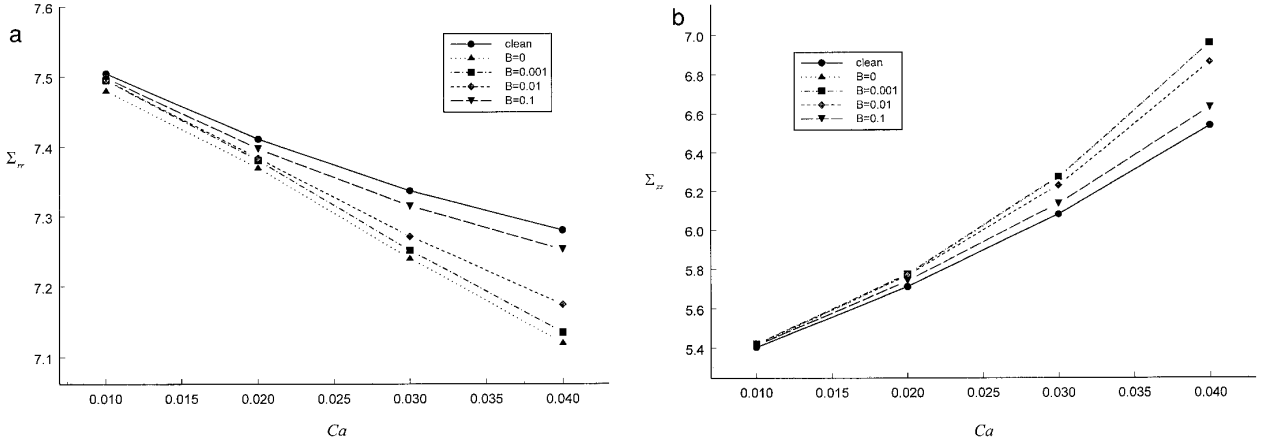

FIG. 13. The volume-averaged stress tensor for $x = 0.1$. (a) Σ_{rr}; (b) Σ_{zz}. (The results for $B = 0$ and $B = 0.001$ superpose.)

3.3. Volume-Averaged Stress Tensor

The drop contribution to the volume-averaged stress tensor (11) is

$$\boldsymbol{\Sigma} = \int_A \mathbf{x}(2H\boldsymbol{\gamma}\mathbf{n} - \nabla_s\gamma)dS. \qquad [32]$$

The radial component Σ_{rr} and axial component Σ_{zz} are shown in Figs. 13 and 14 for low concentrations ($x = 0.1$) and high concentrations ($x = 0.99$), respectively. In dimensional form, the magnitude of $\boldsymbol{\Sigma}$ for $x = 0.99$ is less than that for $x = 0.1$ because of the reduction in surface tension. Since $\boldsymbol{\Sigma}$ is made dimensionless with γ_{eq}/a, the differences not caused by this simple reduction in tension are made apparent.

For $x = 0.1$, as B increases, Σ_{rr} increases and Σ_{zz} decreases monotonically from the insoluble to the clean interface limit. This can be understood in terms of the deformation and the Marangoni stresses. The greater the deformation, the longer the length of the drop and the smaller its cross section. Since deformation decreases with B, cross sections increase, increasing the radial contribution; lengths and Marangoni stresses decrease, decreasing the axial contribution. For $x = 0.5$, similar trends are observed.

For $x = 0.99$, however, the variation of Σ_{rr} is more complex; it first decreases with B from the insoluble limit to a value less than the clean drop result, then increases to reach the clean drop limit. These trends are also well explained by the variations in the breadth of the drop with B. The axial component Σ_{zz} varies monotonically, however, even though the length varies nonmonotonically. This can be understood in terms of the Marangoni stresses, which resist the flow in the axial direction, and which decrease monotonically with B.

3.4. Approximate Mass Balance

For x near unity, Γ develops only perturbative gradients. This observation was used to simplify the mass balance in the insoluble limit, neglecting all fluxes associated with gradients in Γ. The results presented in Fig. 8 suggest that this approx-

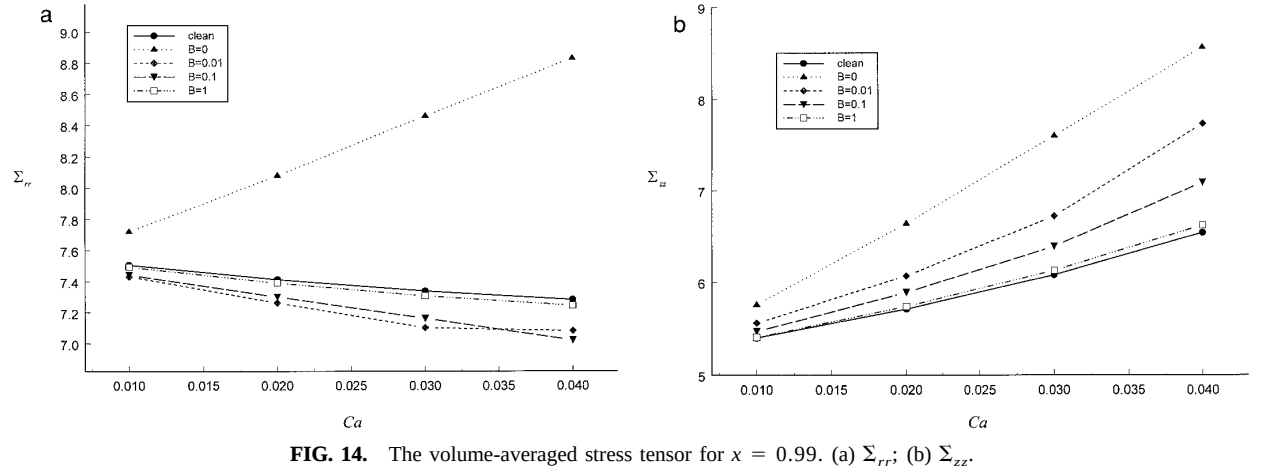

FIG. 14. The volume-averaged stress tensor for $x = 0.99$. (a) Σ_{rr}; (b) Σ_{zz}.

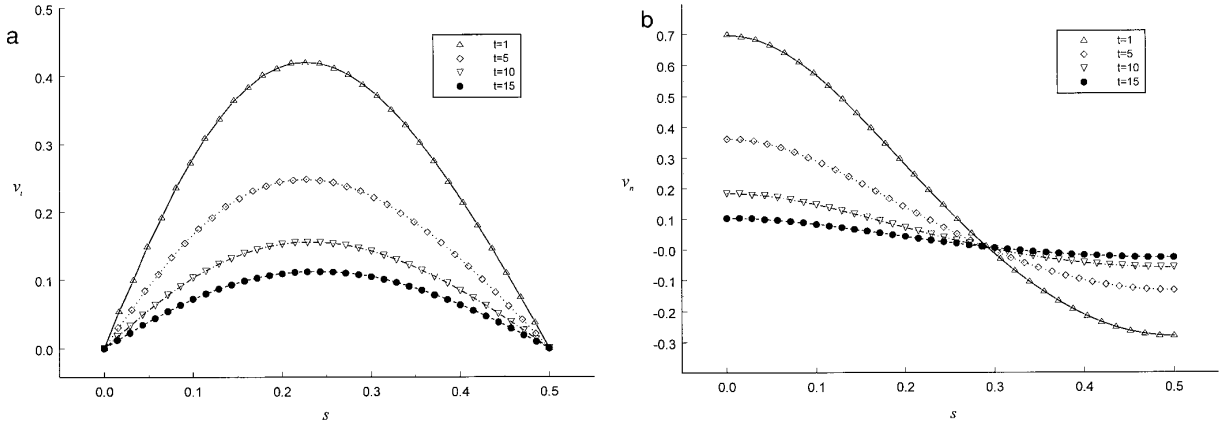

FIG. 15. Comparison of the full and approximate solution of the surface mass balance for $B = 0.01$ for the transient velocities (a) v_t and (b) v_n.

imation is also valid for soluble surfactants at elevated surface coverage. The mass balance is approximated:

$$\frac{1}{\Gamma}\frac{\partial \Gamma}{\partial t} + \nabla_s \cdot (\mathbf{v}_t) + 2H\mathbf{v}_n = \mathrm{Bi}(1 + k)\frac{(1 - \Gamma)}{\Gamma}. \quad [33]$$

This balance was adopted for $\mathrm{Bi} = 0.01$ and compared to the full results. The deformations superpose with the full simulation results in Fig. 12, agreeing to within 0.005% for the lowest Ca studied, and within 1% at the highest Ca studied. The approximate Γ, γ, Marangoni stress, and v_t profiles show similar agreement; they are shown as bold dots in the figures. The implications of this result at steady state are clear: the tangential flux of surfactant at steady state is balanced by mass transfer from the bulk. The faster is this rate of supply, the greater the tangential mobility of the interface. For the unsteady deformation, the evolutions of the tangential and normal velocity profiles also obey this balance (see Fig. 15).

3.5. Moderate Surface Coverage Results: Overestimating E

In Figs. 16–20, the results for $x = 0.5$ are presented for $E = 0.2$ and $E = 8.0$. First consider the insoluble results. According to Eq. [24], the Marangoni stresses are of magnitude $Ex\nabla_s\Gamma/(1 - x)$, or $E\nabla_s\Gamma$. For $E = 0.2$, these stresses are initially weak. The resulting profiles show strong Γ gradients and weak v_t. The drop deformation is dominated by tip stretching, and larger Df result when compared to the clean interface result.

For $E = 8.0$, the initial Marangoni stresses are strong even for small Γ gradients. The velocity is strongly reduced from early in the deformation process. This exaggeration of the coupling between the Marangoni stress and the surface concentration profile strongly alters the drop behavior. The resulting profiles show weak Γ gradients and weak v_t. The drop dilutes as the interface stretches, and smaller Df result when compared to the clean interface result.

Solubility acts to monotonically decrease the deformation for $E = 0.2$ from the insoluble to the clean interface limit; the

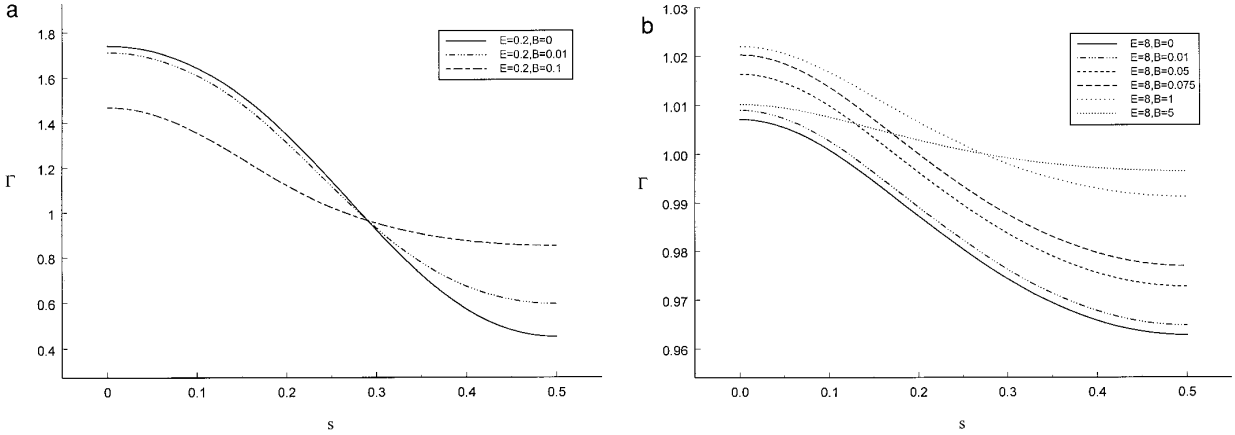

FIG. 16. The surface concentration profile Γ at $\mathrm{Ca} = 0.04$ for $x = 0.5$. All results for $\Lambda = 10^3$. (a) $E = 0.2$, $B = 0$ (insoluble), 10^{-2}, and 10^{-1}; (b) $E = 8.0$, $B = 0$ (insoluble), 10^{-2}, 5×10^{-2}, 7.5×10^{-2}, 1, and 5. Notice that the scales on the figures differ.

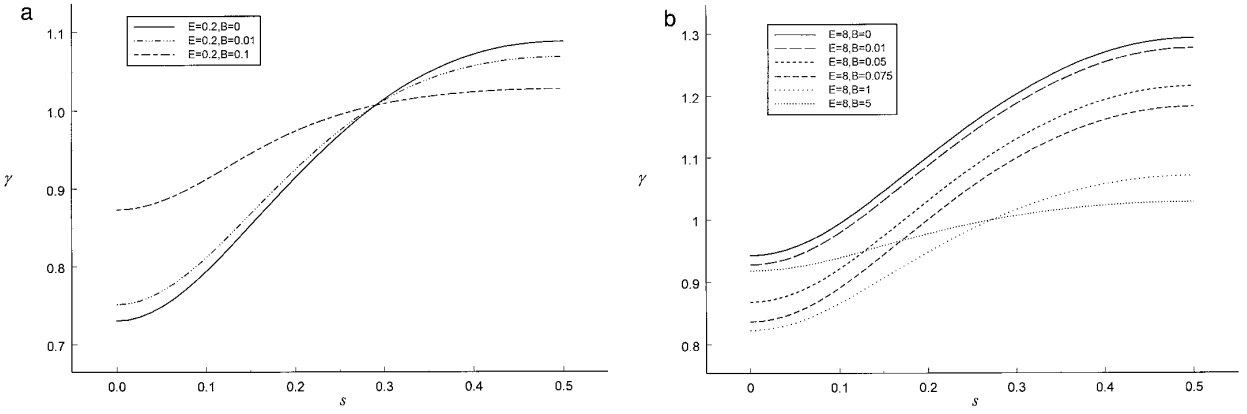

FIG. 17. The surface tension profile γ at Ca = 0.04 for $x = 0.5$. All results for $\Lambda = 10^3$. (a) $E = 0.2$, $B = 0$ (insoluble), 10^{-2}, and 10^{-1}; (b) $E = 8.0$, $B = 0$ (insoluble), 10^{-2}, 5×10^{-2}, 7.5×10^{-2}, 1, and 5. Notice that the scales on the figures differ.

deformations realized are bounded by these limits. For $E = 8.0$, however, the deformations realized are dilution dominated for small B, tip stretching dominated for moderate B, and finally, the same as the clean result for large B. (This simulation also shows nonunique Df for strongly differing B; the Df curves for $B = 0.05$ and $B = 5$ superpose, and differ only slightly from the clean interface result. However, the Γ, γ, Marangoni stress profiles, and v_t profiles differ strongly for $B = 0.05$ and $B = 5$. This nonuniqueness of Df as a function of the surfactant material parameters can occur for any drop whose deformation is dilution dominated in the insoluble limit.)

The adoption of large E (or β_G for the 2-D ideal gas law studies) strongly alters the system behavior. The large Marangoni stresses that develop for small Γ gradients precluded the accumulation of surfactant at the tips in the simulations of Leal and collaborators and the work of Pawar and Stebe, even at low concentrations. This biasing of Γ toward a uniform distribution also forces the drop deformation away from tip stretching in the insoluble limit and allows for the highly nonmonotonic deformation behavior observed with increasing B. Faster mass transfer rates (higher B) are required to recover the clean interface result. Clearly, by altering the deformation behavior, the drop contribution to the system rheology was also influenced.

3.7. Calculation of Controlling Mass Transfer Mechanisms

Most surfactants in aqueous media have diffusivities D of roughly 5×10^{-6} cm^2/s. The differences in their behavior occur because of differing tendencies to adsorb and the rates of adsorption–desorption. Here, the controlling mechanisms for monomeric surfactant transport up to the critical micelle concentration (CMC) are described. Thereafter, the role of micelles in controlling the system behavior is briefly discussed. Langmuir adsorption parameters for a variety of nonionic surfactants are given in Table 1 of Chang and Franses (12). From this table, characteristic magnitudes for Γ_∞ of 2×10^{-10} mol/cm^2, γ_{eq} of 30 dyne/cm, β/α of 10^{10} cm^3/mol, and CMC of 10^{-7} mol/cm^3 are adopted. The viscosities of the dispersed and continuous phases are assumed to be 1 cp. In recent

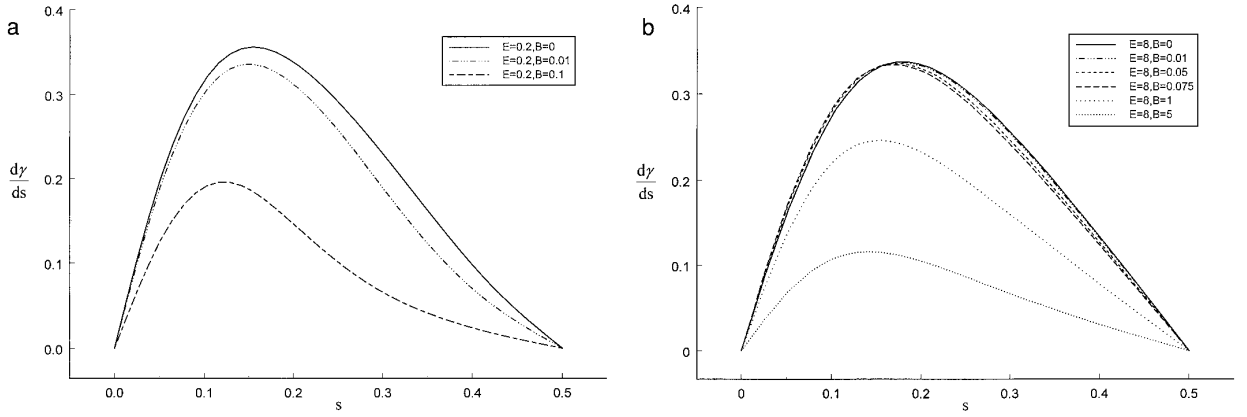

FIG. 18. The Marangoni stress profile at Ca = 0.04 for $x = 0.5$. All results for $\Lambda = 10^3$. (a) $E = 0.2$, $B = 0$ (insoluble), 10^{-2}, and 10^{-1}; (b) $E = 8.0$, $B = 0$ (insoluble), 10^{-2}, 5×10^{-2}, 7.5×10^{-2}, 1, and 5.

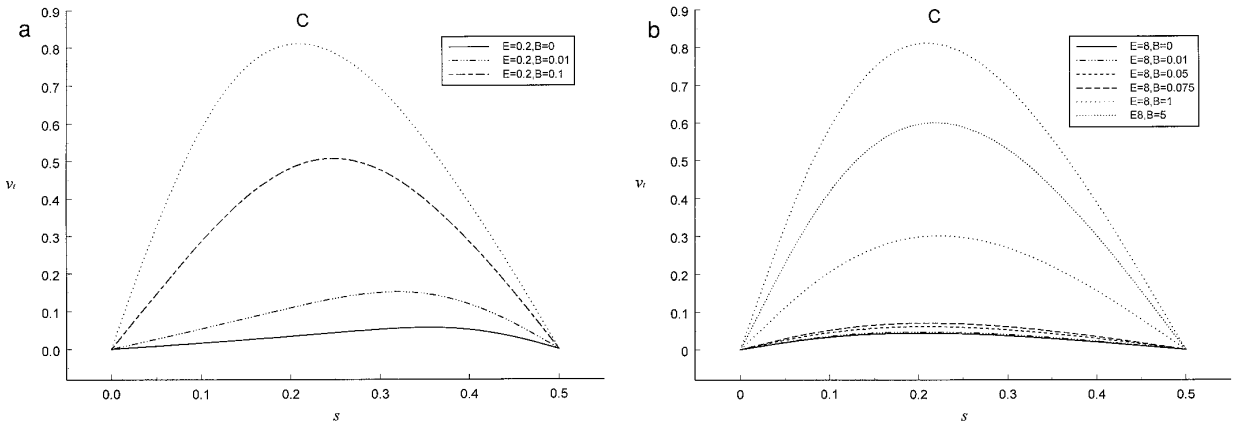

FIG. 19. The tangential surface velocity v_t profile γ at Ca = 0.04 for $x = 0.5$. All results for $\Lambda = 10^3$. (a) $E = 0.2$, $B = 0$ (insoluble), 10^{-2}, and 10^{-1}; (b) $E = 8.0$, $B = 0$ (insoluble), 10^{-2}, 5×10^{-2}, 7.5×10^{-2}, 1, and 5. Notice that the scales on the figures differ.

pendant bubble retraction studies (13), characteristic magnitudes for the desorption coefficient α have been shown to be as slow as 10^{-4} to 10^{-2} s^{-1} for poly-ethoxylated surfactants. Below the range of applicability of the insoluble and sorption controlled analysis is discussed for drops of radius of 1 cm and 1 μm (emulsion-sized drops).

Surfactants behave as if they were insoluble when the mass transfer between the interface and the bulk is slow compared to the surface convective flux. Either the time scales for adsorption–desorption are inherently slow, i.e., Bi $\ll 1$, or the time scales for diffusion flux from the bulk to the interface are slow compared to the surface convective flux, i.e., $(\mathrm{Pe}h)^{-1} \ll 1$. In order for adsorption–desorption to control the surfactant transport, the rate of sorptive exchange must be slow compared to bulk diffusion, i.e., $\mathrm{Bi}(\mathrm{Pe}h) \ll 1$.

Consider a drop of radius $a = 1$ μm. For this small length scale, strong extensional flows must be applied for Ca to be large enough to deform the drop, i.e., for Ca ≥ 0.01, $G \geq 10^5$ s^{-1} are required. At these strain rates, Bi ranges from 10^{-9} to 10^{-7}. The group $1/h\mathrm{Pe}$ ranges from 10^{-7} for extremely dilute solutions to 10^{-4} at the CMC. The group $\mathrm{Bi}(h\mathrm{Pe})$ is also small, so that adsorption–desorptive exchange controls the mass transfer. Note that the extremely small Bi indicate that the mass flux from the bulk is extremely slow compared to the surface convective flux, and the insoluble approximation is valid for drops of this size subject to strong strain rates.

Consider the behavior of larger drops with $a = 1$ cm. In order to attain relevant Ca values, G must be ≥ 30 s^{-1}. For these strain rates, Bi ranges from 3×10^{-6} to 3×10^{-4}. The Peclet number Pe is 6×10^6. For such large bulk Peclet numbers, diffusion boundary layers develop near the drop interface, of thickness $a\mathrm{Pe}^{-1/2}$; the diffusion flux scaling is modified:

$$j_D = -\frac{1}{\mathrm{Pe}^{1/2}h}\,\mathbf{n}\cdot\nabla C|_s. \qquad [34]$$

(This boundary layer thickness applies only if the interface

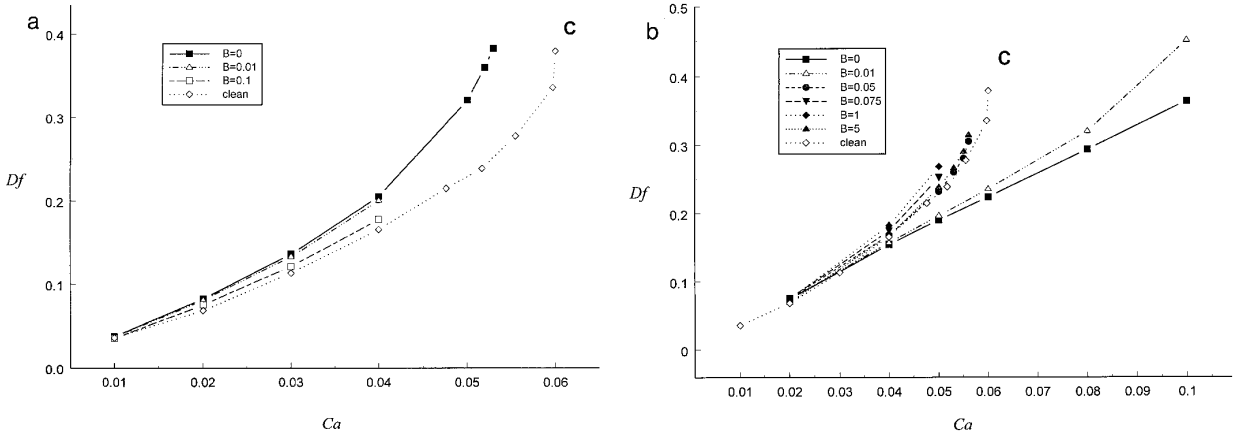

FIG. 20. The deformations Df as a function of Ca for $x = 0.5$. C indicates the surfactant-free case. All results for $\Lambda = 10^3$. (a) $E = 0.2$, $B = 0$ (insoluble), 10^{-2}, and 10^{-1}; (b) $E = 8.0$, $B = 0$ (insoluble), 10^{-2}, 5×10^{-2}, 7.5×10^{-2}, 1, and 5.

is mobile; for immobile interfaces, the exponent on Pe changes to $-\frac{1}{3}$, and the argument which follows must be modified appropriately.) The group $(\mathrm{Pe}^{1/2}h)^{-1}$ ranges in magnitude from roughly 2.0×10^{-4} for trace surfactant concentration to 0.2 at the CMC. (This variation occurs because the adsorption depth decreases as the bulk concentration increases.) Therefore, for concentrations up to an order of magnitude below the CMC, both diffusion and adsorption–desorption are slow enough that the insoluble limit is valid. In order for adsorption–desorption to control the surfactant transport, the group $\mathrm{Bi}(\mathrm{Pe}^{1/2}h)$ must be small; indeed, at the CMC for α of 10^{-4} this group is 10^{-5}; for α of 10^{-2} this group is 10^{-3}. Therefore, for elevated concentrations of monomeric surfactant, the mass transfer is sorption controlled for drops of radius 1 cm.

The scaling arguments for the diffusion flux above are based upon monomeric flux of surfactant. However, most surfactants form micelles, which act as reservoirs of monomer, dissociating if the local concentration is depleted below the CMC. If this timescale is rapid, the monomer concentration will be equal to the CMC. Diffusion is eliminated as a controlling timescale, and the surfactant is adsorption–desorption controlled. (This has been shown to be the case experimentally for a capillary slug flow (14).)

4. CONCLUSIONS AND IMPLICATIONS

The drop behavior is strongly influenced both by the surfactant mass transfer rate and the concentration of surfactant present. At low concentrations, the deformation decreases monotonically with increasing mass transfer rates as the accumulation of surfactant near the tips is eliminated. At high concentrations, deformations vary nonmonotonically as the mass transfer rates increase. The nonmonotonic behavior occurs because adsorption supplies the depleted equatorial region faster than desorption removes surfactant accumulated at the tips. This alleviates any dilution of the drop while still allowing low surface tensions at the tips. Deformations increase from values below the clean case to values greater than the clean case at moderate mass transfer rates.

The drop contribution to the volume averaged stress tensor is strongly influenced by the deformation; drops with greater cross sectional areas have greater radial components to this tensor. The axial components are influenced by both drop length and the magnitude of Marangoni stresses.

At elevated coverage, only perturbative Γ gradients are realized. For insoluble surfactants, Marangoni stresses regulate Γ, forcing it to remain nearly uniform to prevent the local surface concentration from approaching its upper bound. As the mass transfer rates increase, smaller Marangoni stresses are required to keep Γ uniform. Finally, for rapid enough mass transfer, the Γ remains uniform and in equilibrium with the surrounding surfactant solution. The Marangoni stresses approach zero. This suggests a simplified framework for the study of surfactant covered interfaces in the elevated concentration limit in which the Marangoni stress generated is determined by the constraint that it maintain a uniform surface concentration.

REFERENCES

1. Rallison, J. M., *Ann. Rev. Fluid Mech.* **16,** 45 (1984).
2. Stone, H. A., *Ann. Rev. Fluid Mech.* **26,** 65 (1994).
3. Stone, H. A., and Leal, L. G., *J. Fluid Mech.* **220,** 161 (1990).
4. Milliken, W. J., Stone, H. A., and Leal, L. G., *Phys. Fluids A* **5,** 69 (1993).
5. Frumkin, A., *Z. Phys. Chem.* **116,** 446 (1925).
6. Pawar, Y. P., and Stebe, K. J., *Phys. Fluids* **8,** 1738 (1996).
7. Milliken, W. J., and Leal, L. G., *J. Colloid Interface Sci.* **166,** 275 (1994).
8. Eggleton, C. D., Pawar, Y. P., and Stebe, K. J., *J. Fluid Mech.,* in press.
9. Defay, R., and Prigogine, I., "Surface Tension and Adsorption." Wiley, New York, 1966.
10. Pozrikidis, C., "Boundary Integral and Singularity Methods for Linearized Viscous Flows." Cambridge Univ. Press, Cambridge, UK, 1992.
11. Taylor, G. I., *Proc. Roy. Soc. London A* **138,** 41 (1932)
12. Chang, C. H., and Franses, E. I., *Colloids Surf. A* **100,** 1 (1995).
13. Pan, R., Green, J., and Maldarelli, C., *J. Colloid Interface Sci.* **205**, 213 (1998).
14. Stebe, K. J., Lin, S. Y., and Maldarelli, C., *Phys. Fluids A* **3,** 3 (1991).